INVESTIGATION OF PLATINUM-CATALYZED FORMATION OF COBALT NANOPARTICLES BY MIXED POTENTIAL

Mary Donnabelle Lirio Balela-Garcia[1], Shunsuke Yagi[2], and Eiichiro Matsubara[3]

[1] Department of Mining, Metallurgical and Materials Engineering, University of the Philippines,Quezon City, Philippines, e-mail: mdlbalela@gmail.com

[2]Nanoscience and Nanotechnology Research Center, Osaka Prefecture University, Osaka, Japan

[3]Department of Materials Science and Engineering, Kyoto University, Kyoto, Japan

Received Date: February 17, 2014

Abstract

Cobalt (Co) nanoparticles with diameters of 20 to 60 nm were successfully formed by seed-mediated electroless deposition in aqueous solution at room temperature. The formation of Co nanoparticles was investigated by in situ monitoring of mixed potential and deposition rate. Co nanoparticles was produced when the mixed potential was below the oxidation-reduction potential of Co(II)/Co, which coincided with a sharp increase in deposited mass on a gold-sputtered quartz crystal substrate. The mixed potential was positive and Co nanoparticles were not produced without platinum (Pt) addition. Increasing concentration of Pt addition resulted in a decrease in mixed potential and Co nanoparticle diameter. Thus, Pt effectively enhanced Co deposition rate and served as nucleation seeds for Co nanoparticles.

Keywords: Cobalt nanoparticles, Heterogeneous nucleation, Mixed potential, Seed-mediated method

Introduction

Ferromagnetic nanoparticles, such as iron (Fe), cobalt (Co), and nickel (Ni) have been the subject of intensive research for the past two decades due to their unique magnetic and catalytic properties [1-3]. Co is particularly interesting due to the existence of a uniaxial hexagonal close-packed structure besides the face-centered cubic structure, which is important for applications in magnetic recording, catalysis, and biomedicine. Various methods, either physical and chemical, have been explored in order to produce high quality Co nanoparticles. Among the synthetic processes available, liquid-phase processes, such as hydrothermal, polyol, solvothermal, thermal decomposition, reverse-micelle and electroless deposition (chemical reduction) are the most attractive due to their simplicity and low cost [3-6]. Using such methods, it is also possible to produce a large amount of nanoparticles in a single process.

In electroless deposition, metallic nanoparticles are formed by the chemical reduction of metal ions to metal atoms using a reducing agent. Simultaneously, the reducing agent undergoes oxidation leading to the release of electrons. Therefore, electrochemical techniques, such as mixed potential and voltammetry, can be used to investigate the formation of metallic nanoparticles in solution. In this work, Co nanoparticles with diameters of 20 to 60 nm were produced by seed–mediated electroless deposition in an aqueous solution at room temperature. Hydrazine and hexachloroplatinic acid were used as reducing and nucleating agent, respectively. The formation of the nanoparticles was studied by in situ measurement of mixed potential. The mixed potential is defined as the potential wherein the total anodic current

equals the total cathodic current. Additionally, electrochemical quartz crystal microbalance (EQCM) was employed to study the deposition rate of cobalt on an EQCM substrate.

Methodology

The reagents used in this work were analytical grade and supplied by Nacalai Tesque. In a typical experiment, the metal solution and reducing agent solutions were prepared separately. The metal solution was prepared by dissolving 10 mmol Co(II) acetate tetrahydrate, 1.3 x 10^{-3} mmol polyethylene glycol (PEG, Molecular weight = 20,000), and 25 mmol sodium hydroxide (NaOH) in 75 ml distilled water. Nitrogen gas was purged at a rate of 50 ml min^{-1} 30 minutes before the reaction was started. Then, 2.5 x 10^{-2} mmol hexachloroplatinic acid [$H_2Pt(IV)Cl_6$] was added as nucleating agent. The reducing agent solution was prepared by dissolving 100 mmol hydrazine (N_2H_4) in 25 ml deoxygenated distilled water. The two solutions were then mixed vigorously at room temperature.

The morphology of the Co nanoparticles was studied using a field-emission scanning electron microscope (FE-SEM, JSM 6500-F) and a transmission electron microcope (TEM, JEOL JEM 2010). The structure of the Co nanoparticles was investigated in an X-ray diffractometer (MAC Science M03XHF22) with Cr Kα. In situ measurements of the mixed potential, polarization curve, and deposition rate were monitored by a potentiostat/galvanostat (Hokuto Denko Co. Ltd., HA-151) and an electrochemical quartz crystal microbalance (QCA 917). The working and reference electrode were 9MHz AT-cut Au-sputtered quartz crystal substrate and a Ag/AgCl electrode (Horiba 2565-10T), respectively. A Pt sheet was used as a counter electrode.

Results

Figure 1a shows the change in mixed potential with time during seed-mediated electroless deposition of Co nanoparticles for pH 12 at room temperature. At the start of the reaction, the mixed potential is more positive than the oxidation-reduction of Co(II)/Co ($E_{Co(II)/Co}$ = –0.62 V). At less than 10 min reaction, the mixed potential shifts below $E_{Co(II)/Co}$, which coincides with the observed change in the solution color from pink to black. The mixed potential then remains below $E_{Co(II)/Co}$ until the end of the reaction at 1 hr. The corresponding change in the deposited mass is shown in Figure1b. At the early stages of the reaction, Δm gradually increases. Since the mixed potential is above the $E_{Co(II)/Co}$ and no Co deposition should occur, it is apparent that an intermediate phase, possibly Co(II) hydroxide, adheres on the surface of the electrode at the beginning. However, broad hexagonal close-packed (hcp) and face-centered cubic (fcc) Co peaks together with diffused $Co(OH)_2$ peaks at 57.7 ,°58.9°, and 80.2° are present in the XRD pattern of the product at 5 min reaction as in Figure2a. This suggests that minute Co deposition possibly occurs at the early stage of the stage, which corresponds with EQCM measurement in Figure1b. As the reaction proceeds, Δm abruptly increases at about 20 min. This point coincides with the lowest value of mixed potential in Figure1a.

Figure 2 shows the XRD patterns of the precipitates obtained at different reaction times. At longer reaction times (> 10 min), diffraction peaks are only attributed to both hexagonal close-packed (hcp) and face-centered cubic (fcc) Co structures. This suggests that strong Co deposition occurs after about 10 min as indicated by the change in the color of the solution.

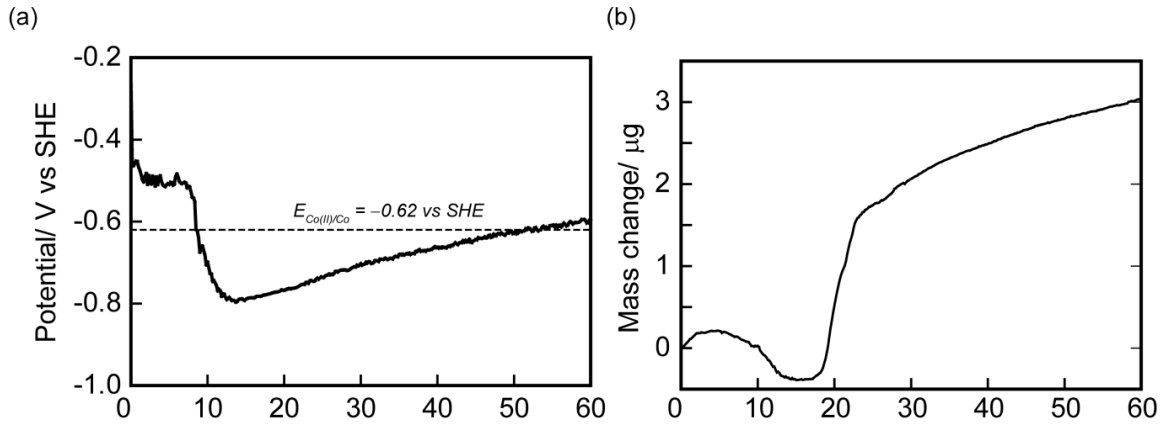

Figure 1. Changes in (a) mixed potential and (b) deposited mass during electroless deposition of Co at pH 12 in an aqueous solution at room temperature

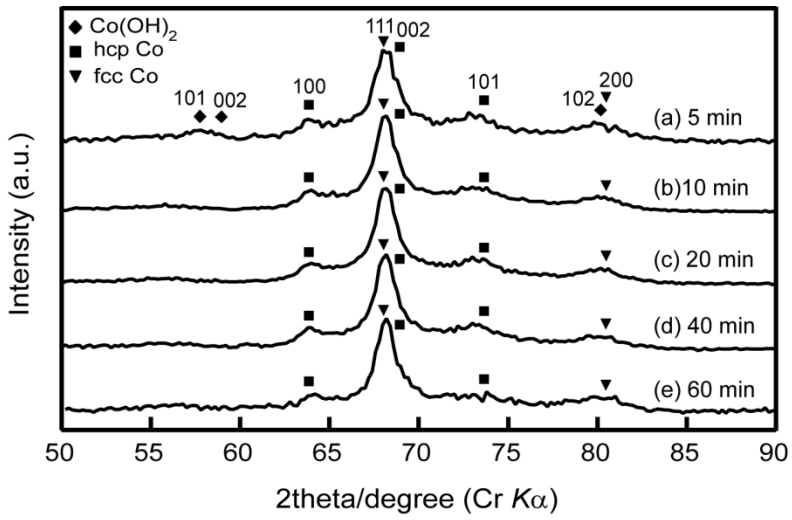

Figure 2. XRD patterns of Co products prepared after (a) 5, (b) 10, (c) 20, (d) 40 and (e) 60 minutes reaction times

Discussion

Several cathodic and anodic partial reactions occur concurrently in the solution during the electroless deposition of Co. The primary cathodic partial reactions are Pt deposition, Co deposition, and H_2 generation, while the primary anodic partial reaction is N_2H_4 oxidation to N_2 gas and H_2O. The oxidation-reduction potential of the Pt(IV)/Pt redox pair is more positive than the values for Co(II)/Co and H_2O/H_2 redox pairs. Thus, Pt(IV) ions from the nucleating agent H_2PtCl_6 are first reduced by the reducing agent N_2H_4 to form very small Pt nanoparticles that act as heterogeneous nucleation sites for Co.

From thermodynamics, Co deposition will only occur when the mixed potential is less than the oxidation-reduction of Co(II)/Co redox pair and the activity of Co^{2+} aquo ions in equilibrium with abundant $Co(OH)_2$ at pH 12. Thus, when the mixed potential shifts below

$E_{Co(II)/Co}$ before 10 min reaction, large concentration of Co atoms preferentially deposits on the surface of Pt nanoparticles. Co nanoparticles are then precipitated in the solution and Δm increases sharply. A significant amount of gas due to H_2 generation and oxidation of N_2H_4 is simultaneously released with the precipitation of Co nanoparticles. N_2H_4 is thereby consumed by the reaction, leading to the decrease in the anodic current density. As a result, the mixed potential increases as more Co nanoparticles are produced.

Since strong Co deposition only occurs after about 10 min in the reaction, the initial increase in Δm is attributed to the deposition of minute Co nanoparticles and mostly to the adhesion of the intermediate phase $Co(OH)_2$. To further investigate the deposition reaction of Co, the cathodic polarization curve coupled with the effective mass change was measured in an aqueous solution with 87 mM Co(II) acetate, 0.22 M NaOH, and 0.10 M sodium sulfate as supporting electrolyte. The solution had a total volume of 115 ml with a pH 12. The cathodic polarization curve measured at 1 mV s^{-1} from the rest potential of 0.20 V up to –1.0 V against SHE is shown in Figure 3a. The cathodic current starts to flow at about –0.73 V vs SHE. This is more negative than the calculated oxidation-reduction potentials for Co(II)/Co and H_2O/H_2 redox pairs at pH 12. This indicates that both Co deposition and H_2 evolution reactions occurs simultaneously, leading to an increase in the pH near the surface of the electrode. Consequently, the deposition of $Co(OH)_2$ is promoted.

The mass change during cathodic polarization is shown in Figure 3b. A positive Δm of about 1.0 x 10^{-2} μg is observed instantaneously after immersing the working electrode in the Co(II) solution. While the current density remains zero, Δm gradually increases as the potential is changed from –0.20 to –0.73 V. This suggests that non-faradaic deposition occurs before Co deposition, which supports the EQCM measurement in Figure 1b. As the potential is further decreased below –0.80 V, Δm sharply increases. This implies faster Co deposition at more negative potentials.

Figure 4 shows the mixed potentials measured in aqueous solutions containing different concentrations of nucleating agent, H_2PtCl_6. Without H_2PtCl_6, the mixed potential is unstable, possibly due to very small cathodic and anodic current densities during the reaction. Their average values are plotted in Figure 4a, which is obviously much higher than $E_{Co(II)/Co}$ throughout the reaction. As a result, no Co nanoparticles are formed even after 2 h. In contrast, the mixed potential shifts more negatively with an increase in the concentration of H_2PtCl_6, and the reduction of Co(II) occurs faster. In the presence of 2.2 x 10^{-2} mM H_2PtCl_6, the mixed potential drops to $E_{Co(II)/Co}$ about 7 min after the addition of the reducing agent N_2H_4. The color of the solution then changes to black. Adding more H_2PtCl_6 results in an instantaneous drop of the mixed potential below $E_{Co(II)/Co}$, and a spontaneous change in the color of the solution. Because of the acceleration of the reaction rates with higher amounts of H_2PtCl_6, it is plausible that the Pt nanoparticles formed from H_2PtCl_6 act as catalysts for Co deposition, as well as nucleation sites for Co nanoparticles [7-11].

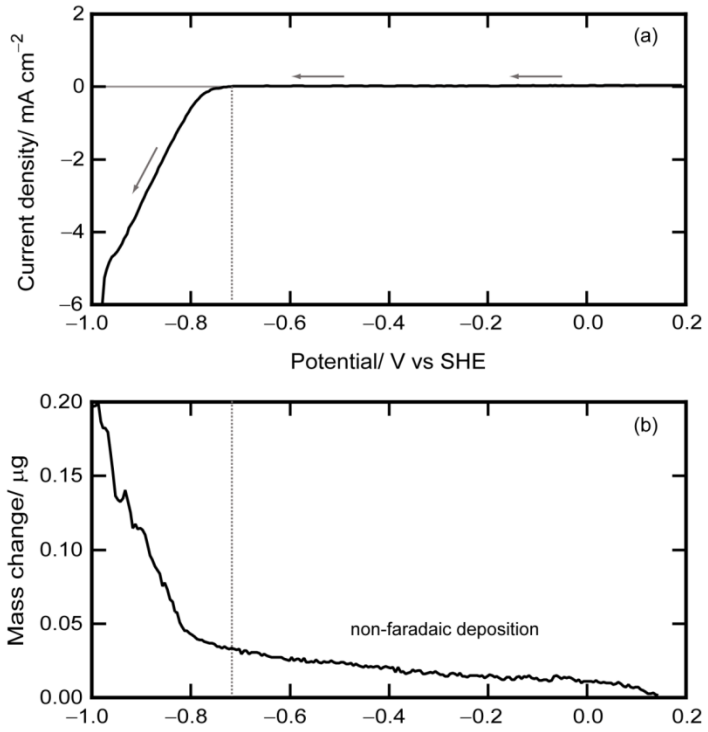

Figure 3. (a) Cathodic polarization curve and the (b) effective mass change measured on a Au-sputtered QCM substrate

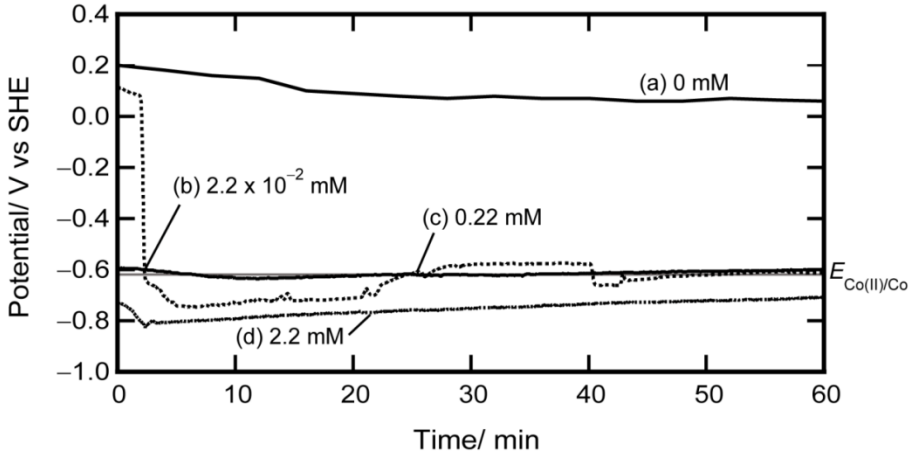

Figure 4. Change in mixed potential during electroless deposition of Co in an aqueous solution at room temperature with (a) 0, (b) 2.2 x 10^{-2}, (c) 0.22, and (d) 2.2 mM H_2PtCl_6

To elucidate the influence of H_2PtCl_6 on the reaction rate, the change in mixed potential during Pt deposition is observed. Except for Co(II) acetate, the aqueous solutions contain the same concentration of reactants as those used during the synthesis of Co nanoparticles (0.22 M NaOH, 1.1 mM PEG, and 0.87 M N_2H_4). Figure 5 shows lower mixed potential with an increase in the concentration of H_2PtCl_6. N_2H_4 is catalytically oxidized on the surface of Pt nanoparticles [12]. Therefore, the decrease in the mixed potential at higher concentration of

H_2PtCl_6 is explained by considering that the mixed potential is mainly controlled by a change in the current density for N_2H_4 oxidation. The oxidation of N_2H_4 is generally slow at room temperature, but the addition of H_2PtCl_6 accelerates the reaction due to the catalytic activity of the Pt nanoparticles. The anodic current density therefore increases, which lowers the mixed potential. At the same time, the reduction of Co(II) occurs more readily owing to the enhanced oxidation of N_2H_4 at higher amounts of H_2PtCl_6. As a result, small Co nanoparticles are immediately formed as shown in Fig. 6. This shows that the nucleating agent apparently works as nuclei of Co nanoparticles [7,13]. The smallest Co nanoparticles of about 24 nm in mean diameter are prepared with the addition of 2.2 mM H_2PtCl_6. The relative standard deviations of the sample size are about 12 - 16 %, which indicates quite narrow size distributions.

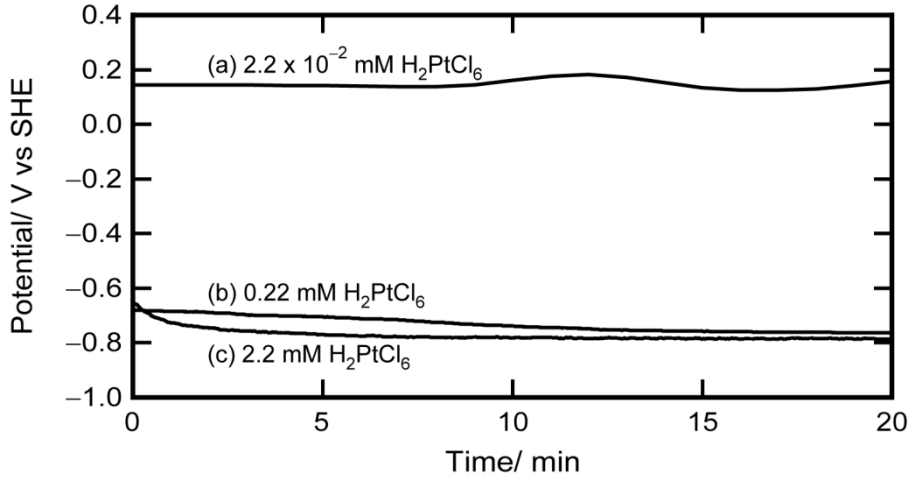

Figure 5. Change in mixed potential during electroless deposition of Pt in an aqueous solution at room temperature using (a) 2.2 x 10^{-2}, (b) 0.22, and (c) 2.2 mM H_2PtCl_6

Conclusions

It was demonstrated that in situ measurement of mixed potential in combination with electrochemical quartz crystal microbalance can be used to investigate the seed-mediated synthesis of Co nanoparticles in aqueous solution at room temperature. Co deposition occurs when the mixed potential is below $E_{Co(II)/Co}$, which is supported by an increase in the deposited mass measured by EQCM. At the early stages of the reaction, non-faradaic deposition takes place due to the high pH near the electrode surface. However, the formation of minute Pt nanoparticles from the nucleating agent accelerates the oxidation of the reducing agent N_2H_4. Consequently, the mixed potential decreases and Co deposition is initiated.

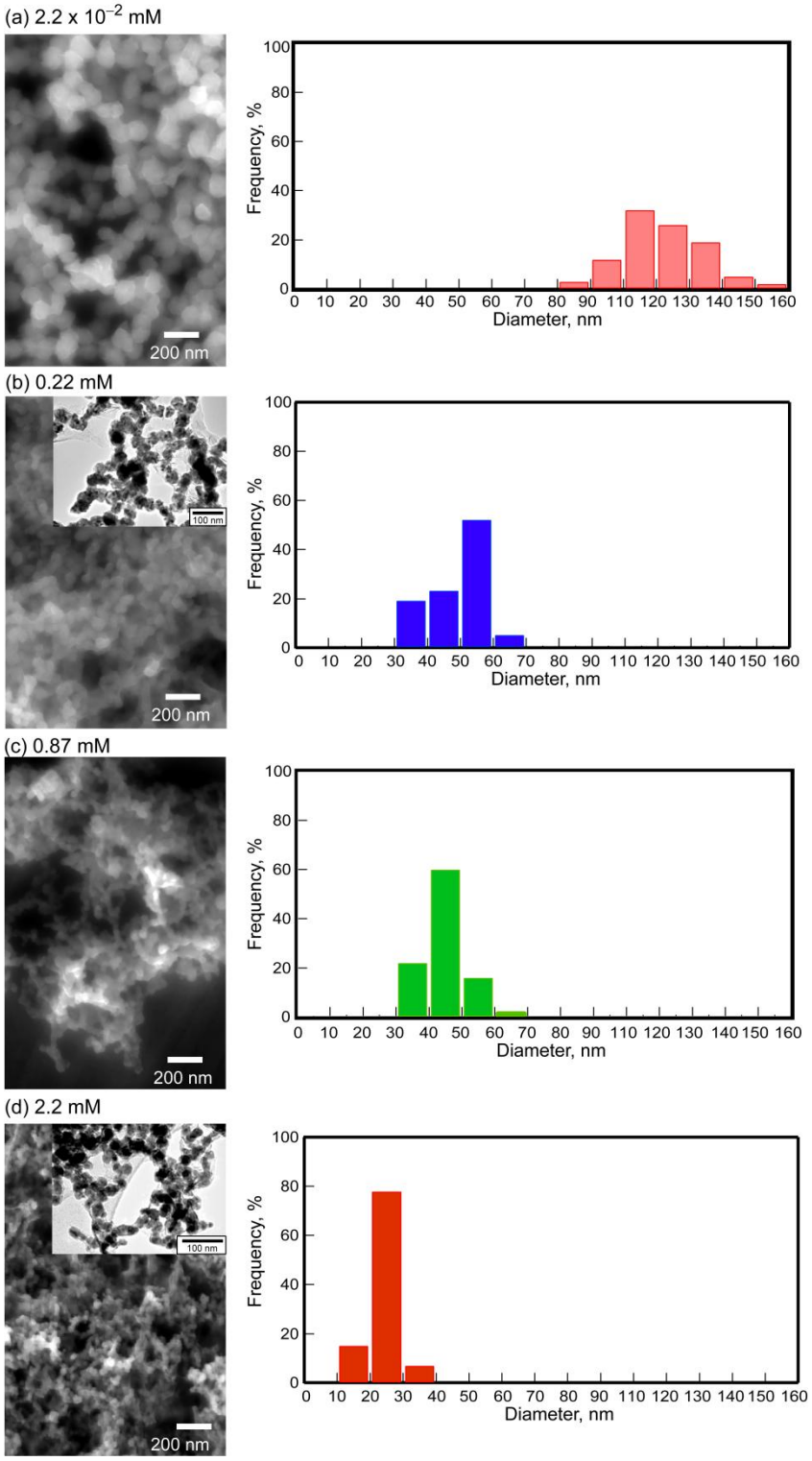

Figure 6. SEM and TEM images of Co nanoparticles prepared using (a) 2.2 x 10^{-2}, (b) 0.22, (c) 0.87, and (d) 2.2 mM H_2PtCl_6 nucleating agent. The mean particle size is (a) 112, (b) 54, (c) 40, and (d) 24 nm

References

[1] G. Cao, *Nanostructures and Nanomaterials: Synthesis, Properties and Applications*, Imperial College Press, London, 2004.

[2] S.P. Gubin, Y.A. Koksharov, G.B. Khomutov, and G.Y. Yurkov, "Magnetic nanoparticles: Preparation, structure and properties," *Russian Chemical Review*, Vol. 74, pp. 489, 2005.

[3] G.B. Sergeev, *Nanochemistry*. Elsevier, Amsterdam, 2006.

[4] P. Tartaj, M.P. Morales, S. Veintemillas-Verdaguer, T. Gonzalez-Carreno, and C.J. Serna, "The preparation of magnetic nanoparticles for applications in biomedicine," *Journal of Physics D: Applied Physics*, Vol. 36, pp. R182, 2003.

[5] Q. Liu, X. Guo, J. Chen, J. Li, W. Song, and W. Shen, "Cobalt nanowires prepared by heterogeneous nucleation in propanediol and their catalytic properties," *Nanotechnology*, Vol. 19, pp. 365608, 2008.

[6] G. Viau, C. Garcia, T. Maurer, G. Chaboussant, F. Ott, Y. Soumare, and J.-Y. Piquemal, "Highly crystalline cobalt nanowires with high coercivity prepared by soft chemistry," *Physica Status Solidi A*, Vol. 206, pp. 663, 2009.

[7] M.D.L. Balela, S. Yagi, and E.E. Matsubara, "Electroless deposition of ferromagnetic cobalt nanoparticles in propylene glycol," *Journal of Electrochemical Society*, Vol. 156, pp. E139, 2009.

[8] M.D.L. Balela, S. Yagi, and E. Matsubara, "Room-temperature synthesis of cobalt nanoparticles by electroless deposition in aqueous solution," *Electrochemical Solid-State Letters*, Vol. 13, pp. D4, 2010.

[9] M.D.L. Balela, S. Yagi, and E. Matsubara, "Room-temperature synthesis of cobalt nanoparticles in aqueous solution," *ECS Transactions*, Vol. 28, pp. 29, 2010.

[10] E. Gileadi, *Electrode Kinetics for Chemists, Chemical Engineers, and Materials Scientists*, Wiley-VCH, Inc., New York, 1993.

[11] W.M. Latimer, *The Oxidation States of the Elements and their Potentials in Aqueous Solutions*, 2nd Edition, Prentice-Hall, Englewood Cliffs, NJ, 1959.

[12] M. Grzelczak, J. Perez-Juste, B. Rodriguez-Gonzales, M. Spasova, I. Barsukov, M. Farle, and L.M. Liz-Marzan, "Pt-catalyzed growth of Ni nanoparticles in aqueous ctab solution," *Chemistry of Materials*, Vol. 20, pp. 5299, 2008.

[13] T. Sugimoto, *Monodispersed Particles*, Elsevier, Amsterdam, 2001.